Polymer 50 (2009) 336–346

Contents lists available at ScienceDirect

Polymer

journal homepage: www.elsevier.com/locate/polymer

Dissipative particle dynamics study on the phase morphologies of the ultrahigh molecular weight polyethylene/polypropylene/poly(ethylene glycol) blends

Jing-Gang Gai [a,b], Hui-Lin Li [a,*], Cornelius Schrauwen [b], Guo-Hua Hu [b,c,**]

[a] State Key Laboratory of Polymer Materials Engineering, Polymer Research Institute of Sichuan University, Chengdu, Sichuan 610065, People's Republic of China
[b] Laboratory of Chemical Engineering Sciences, Nancy-Université, CNRS-ENSIC-INPL, 1 rue Grandville, BP 20451, 54001 Nancy, France
[c] Institute Universitaire de France, Maison des Universités, 103 Boulevard Saint-Michel, 75005 Paris, France

ARTICLE INFO

Article history:
Received 16 April 2008
Received in revised form 3 October 2008
Accepted 15 October 2008
Available online 1 November 2008

Keywords:
Dissipative particle dynamics
UHMWPE
Phase separation

ABSTRACT

The dissipative particle dynamics (DPD) simulation method has been used to study mesophase formation of the binary UHMWPE/PP and ternary UHMWPE/PP/PEG blends. The effects of shear rates and volume fractions of each of the blend components on end-to-end distances of UHMWPE, diffusivities and mesoscale morphologies of the blends have been investigated in detail. As compositions of the UHMWPE/PP and UHMWPE/PP/PEG blends vary, the mesoscale simulations have predicted the ordered structures with defined morphologies of lamellas, perforated lamellas, hexagonal spheres, and body-centered-cubic spheres. Micelle-like melted structures between totally disordered and the ordered phases have also been found in the UHMWPE/PP (10/90) blends. Immiscibility property of UHMWPE, PP and PEG induces the phase separation and exhibits different mesoscpic morphologies at different shear rates and volume fractions. Taking the shear rates dependence of mesophase into account, the change in morphology of the UHMWPE/PP/PEG blends with shear rate is also well studied in this work. As a function of PP concentration, the end-to-end distances of UHMWPE are found to decrease with the increase of PP concentration. This effect is more prominent for a high amount of PP.

1. Introduction

UHMWPE and its composites are widely used as bearing components, gears, guide rails and medical materials in total joint replacement [1–4] because of their excellent friction and wear characteristics, bio-compatibility, chemical stability, effective impact load damping and mechanical properties [5]. Its application, however, is limited due to its poor processability.

In the last thirty years, the development of high-performance UHMWPE composites often involves the use of a low molecular weight solvent to reduce its high entanglement density in forming the final products [6–9]. The apparent disadvantage of such processes is the use of organic solvents, which are difficult to recycle and to remove. Another effective way to reduce the melt viscosity is to dilute the UHMWPE with conventional PE (HDPE, LDPE, and LLDPE) that generally has a lower average molecular weight [10,11]. It is, nevertheless, not without an attendant disadvantage in the process since effective amounts of intermediate molecular weight polyethylene causes a remarkable decrease in some of the most desirable properties. For example, the original excellent mechanical properties are not easy to maintain.

Our previous investigation indicated that UHMWPE with 10–30% polypropylene (PP) can be extruded by a conventional single extruder, and its mechanical and tribological properties were as good as or even better than that of pure UHMWPE [12]. Unfortunately, the melt fluidity of the UHMWPE/PP blend is still low, for example, the melt flow rate of the UHMWPE/PP (75/25) was 0.66 g/10 min under the condition of 230 °C and 21.6 kg load. Our further studies indicated that the addition of a small amount of PEG could significantly reduce the die pressure and melt viscosity of the UHMWPE/PP blends [13].

Computer simulations have provided valuable microscopic and mesoscopic insights into the phase morphology [14–16] and the interfacial behaviors of the immiscible molecules, such as phase separation, the interface thickness and the interface molecular orientation, which significantly influence rheological and mechanical properties of materials [17–22]. The dissipative particle dynamics (DPD) method developed by Hoogerbrugge and Koelman [17,23] is a mesoscopic simulation technique for complex fluids that can study systems over larger length and time scales than classical

* Corresponding author. Tel.: +86 28 85406333; fax: +86 28 85402465.
** Corresponding author. Laboratory of Chemical Engineering Sciences, Nancy-Université, CNRS-ENSIC-INPL, 1 rue Grandville, BP 20451, 54001 Nancy, France. Tel.: +33 383175339; fax: +33 383322975.
E-mail addresses: nic7703@scu.edu.cn (H.-L. Li), hu@ensic.inpl-nancy.fr (G.-H. Hu).

0032-3861/$ – see front matter
doi:10.1016/j.polymer.2008.10.020

molecular dynamics. Español and Warren have added the fluctuation–dissipation relation in DPD [24] while together with Groot, the latter have also applied a coarse-grained method to build the mapping relation of force parameters in DPD with the energy parameters in Flory–Huggins theory [18].

DPD method has been successfully applied to polymeric systems by introducing bead-spring type models [25–27], and it is particularly suitable to investigate the microphase separation and rheological properties of block copolymers and polymer blends [22,28,29]. As an example of application, Groot and Warren tested the DPD model on calculating the interfacial tension between incompatible components and derived a master curve for that in terms of the Flory–Huggins χ parameter. Comparing the curve with the experimental data on polystyrene/polymethyl methacrylate (PS/PMMA) interfacial tension [30], they found that DPD simulation results can be used to quantitatively predict some properties of the real systems [19,31–37]. Furthermore, Wijmans et al. have constructed a master equation by which one can make a quantitative comparison between the simulations and the experimental data [38]. Groot and Rabone showed that by systematically coarse graining, one may obtain the parameters in DPD directly from experimental interaction parameters [39]. Studies with DPD on the influence of phase morphology and interfacial behavior on the rheological behavior of polymer blends are scarce, however. As a result, in this work a DPD simulation that focuses on the phase morphologies, end-to-end distances, density distributions and diffusivities of the ternary UHMWPE/PP/PEG blends is carried out to provide useful information on the processing of UHMWPE with tailored properties. Concentrations of PP and components of the UHMWPE/PP/PEG blends as well as shear rates are taken into account in the simulations.

2. Method

2.1. DPD method

In the DPD method, a group of atoms or a volume of fluid, which is large on the atomistic scale but is still macroscopically small, is represented by beads. In the present work, the interacting beads' time evolution obeys Newton's equations of motion [18]:

$$\frac{\mathrm{d}\boldsymbol{r}_i}{\mathrm{d}t} = \boldsymbol{v}_i;\ \frac{\mathrm{d}\boldsymbol{v}_i}{\mathrm{d}t} = \boldsymbol{f}_i \tag{1}$$

where $\boldsymbol{r}_i$ and $\boldsymbol{v}_i$ are the position and velocity of the ith particle, respectively. All the masses are normalized to 1 for simplicity, and the force acting on a particle is a sum of three pairwise contributions: a conservative force $\boldsymbol{F}^C$, a dissipative force $\boldsymbol{F}^D$, and a random force $\boldsymbol{F}^R$, i.e.,

$$f_i = \sum_{j\neq i}(\boldsymbol{F}_{ij}^C + \boldsymbol{F}_{ij}^D + \boldsymbol{F}_{ij}^R) \tag{2}$$

where the sum runs over all other particles within a certain cutoff radius r_c. As this is the only length-scale in the system, we use the cutoff radius as our unit of length, $r_c = 1$. The different parts of the forces are given by:

$$F_{ij}^C = \begin{cases} a_{ij}(1-r_{ij})e_{ij} & (r_{ij}<1) \\ 0(r_{ij}\geq 1) \end{cases} \tag{3}$$

$$F_{ij}^D = -\gamma\omega^D(r_{ij})(v_{ij}e_{ij})e_{ij} \tag{4}$$

$$\boldsymbol{F}_{ij}^R = \boldsymbol{\sigma}\omega^R(r_{ij})\xi_{ij}\Delta t^{-1/2}e_{ij} \tag{5}$$

where $\boldsymbol{r}_{ij} = \boldsymbol{r}_i - \boldsymbol{r}_j$, $r_{ij} = |\boldsymbol{r}_{ij}|$, $\boldsymbol{e}_{ij} = \boldsymbol{r}_{ij}/r_{ij}$, and $\boldsymbol{v}_{ij} = \boldsymbol{v}_i - \boldsymbol{v}_j$. ξ_{ij} is a random number with zero mean and unit variance. $\boldsymbol{a}_{ij}$ is a constant which describes the maximum repulsion between interacting beads. ω^D and ω^R, respectively represent r-dependent weight functions for the dissipative and random forces, and vanish for $r > r_c = 1$. Unlike the conservative force, the weight functions $\omega^D(r_{ij})$ and $\omega^R(r_{ij})$ of the dissipative and random forces couple together to form a thermostat. Español and Warren have shown that there is fluctuation–dissipation theorem in the dissipative force and the random force [24]:

$$\omega^D(r) = \left[\omega^R(r)\right]^2\cdot\sigma^2 = 2\gamma k_B T \tag{6}$$

the weight functions are chosen simply by [18]:

$$\omega^D(r) = \left[\omega^R(r)\right]^2 = \begin{cases} (1-r)^2(r<1) \\ 0(r\geq 1) \end{cases} \tag{7}$$

for detail comments on them, refer to Groot and Warren's work [18].

The soft-sphere interactions of DPD can be mapped onto Flory–Huggins theory through the χ parameter [18,19]. If the system has i and j components or beads interacting with each other and if one chooses $a_{ii} = a_{jj}$ and assumes that $\rho_i + \rho_j$ is approximately constant, then, according to Groot and Warren [18], the mapping relation is:

$$\chi = \frac{2\alpha(a_{ij}-a_{ii})\left(\rho_i+\rho_j\right)}{k_B T} \tag{8}$$

where α is a parameter related to the pair-correlation function $g(r)$, which is expressed as a function of the reduced co-ordinate $r = \mathbf{r}/r_c$, and $\rho_i + \rho_j = \rho$ is the density of the system.

2.2. Simulation parameters and model construction

The conservative interaction strength α_{ij} was chosen according to the linear relation with Flory–Huggins χ parameters [18] for polymers:

$$\alpha_{ij} = \alpha_{ii} + 3.27\chi_{ij} \quad (\rho = 3) \tag{9}$$

The interaction parameter between the same type beads α_{ii} equals 25. In the present study, we estimated χ of UHMWPE/PP, UHMWPE/PEG and PP/PEG pairs from the solubility parameters by Eq. (9) [40]:

$$\chi = \frac{V_{\mathrm{bead}}(\delta_i-\delta_j)^2}{RT} \tag{10}$$

where V_{bead} is the average molar volume of the beads, and δ_i and δ_j are the solubility parameters of beads i and j, respectively [41]. The DPD simulations of the UHMWPE/PP/PEG blends were performed in a cell of size $30\times30\times30$ (without shear flow) or $50\times20\times20$ (under shear flow), with the bead density $\rho = 3$. Periodic boundary conditions were applied and the shear flow was simulated by means of Lees–Edwards boundary conditions. For convenience, the particle mass m, and k_BT were all taken as unit. The time step Δt was taken as 0.05 [42], and adjacent particles in the polymer chain interacted via a linear spring with a harmonic spring constant of 4.0, according to Groot and Liu [19,32,43–45]. Besides, the friction coefficient γ was chosen as 4.5 [15,45]. A total of 2×10^5 DPD steps were carried out for a DPD simulation in this work. All the DPD simulations were performed using the Materials Studio software package [46]. The DPD analysis module allows one to analyze a mesoscale trajectory created by DPD. The module can return a histogram of the end-to-end distance of a molecule for each of the frames selected. The histogram is accumulated over all molecules and all steps up until the previous frame. The final returned result is the corresponding radial distribution, which is the histogram divided by the total bin count and the volume of each bin [47]. In

Table 1
The characteristic ratios, molecular weights and the corresponding DPD chain lengths of the species in the UHMWPE/PP/PEG blends.

Species	M_p	C_n	N_{DPD}
UHMWPE	2.5×10^6	7.7	11,605
PP	7.3×10^4	6.9	250
PEG	5.5×10^4	5.0	250

this paper, the end-to-end distance corresponding to the most probable distribution was used for representing the end-to-end distance of a polymer chain [48].

The number of beads in each mesoscale molecule is determined by the degree of polymerization and the characteristic ratio (C_n) of

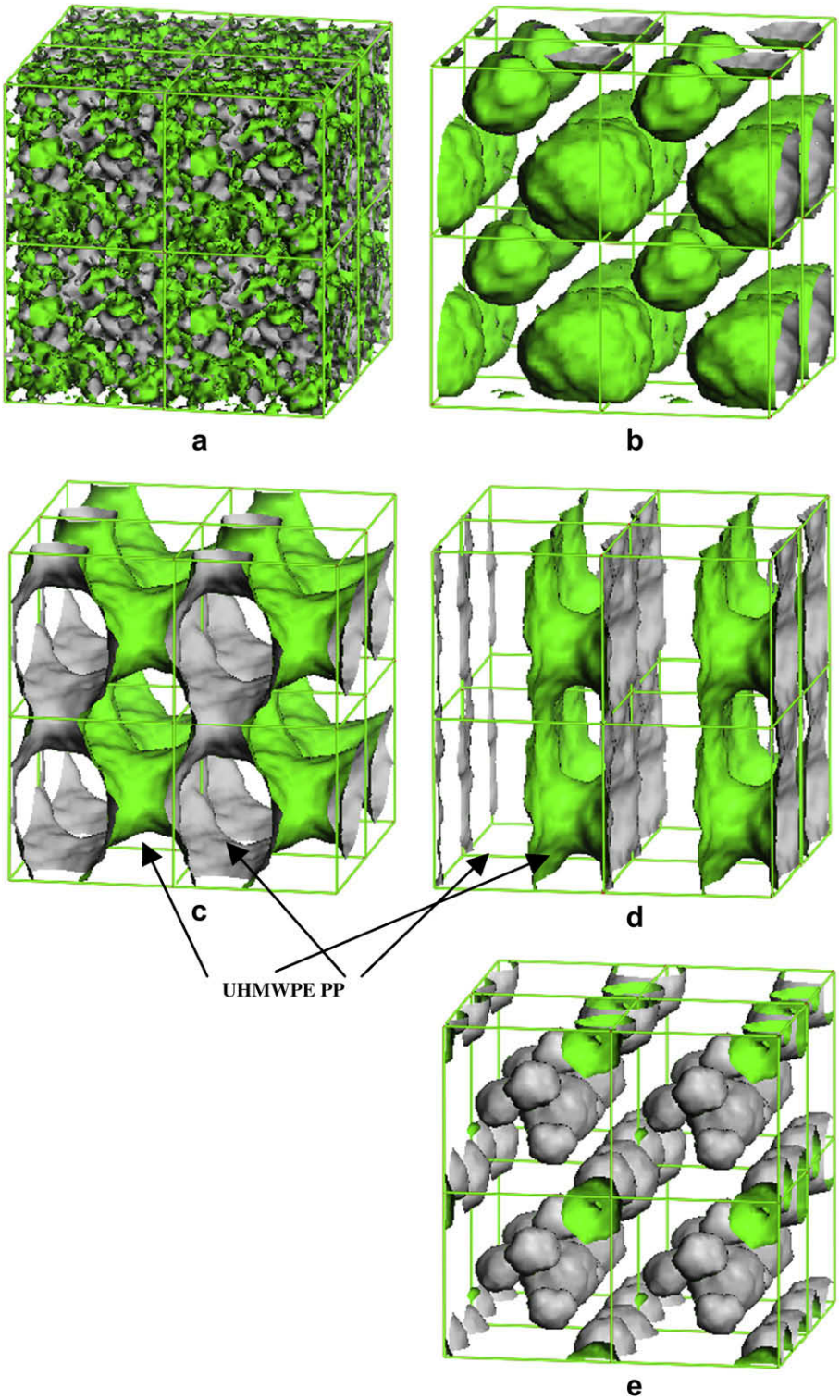

Fig. 1. Iso-density surfaces of PP for the UHMMPE/PP blends obtained after 2×10^5 steps DPD simulation. The outward surfaces of PP phases are colored with green, and the rests are UHMMPE phases. Each system contains 8.1×10^4 DPD beads: (a) UHMMPE/PP (90/10), (b) 70/30, (c) 50/50, (d) 30/70 and (e) 10/90. (For interpretation of the references to colour in this figure legend, the reader is referred to the web version of this article.)

the polymer. The expression for the DPD chain length (N_{DPD}) is [48,49]:

$$N_{DPD} = \frac{M_p}{M_m C_n} \tag{11}$$

where M_p is the polymer molecular weight, M_m is the monomer weight and C_n is the characteristic ratio. Characteristic ratios were obtained by using quantitative structure property relationship (QSPR) methods [48,50]. The characteristic ratios, molecular weights and the corresponding DPD chain lengths of the species in the UHMWPE/PP/PEG blends are listed in Table 1.

Both the UHMWPE/PP binary blends and the UHMWPE/PP/PEG ternary blends evolve from random disordered states in the mesoscopic dynamics simulations, where the polymers are in a homogeneous melted state. During the temperature relaxation, we observed the mesophase separation process and ordered phase generation into mesoscopic domains. In this work a transition from a homogeneous melt state of chains to a heterogeneous melt of ordered mesophases-separated domains is defined to be an order–disorder transition (ODT). The description of each binary or ternary blend generates a coarse-grained system sufficiently large to identify the formation of ordered structures.

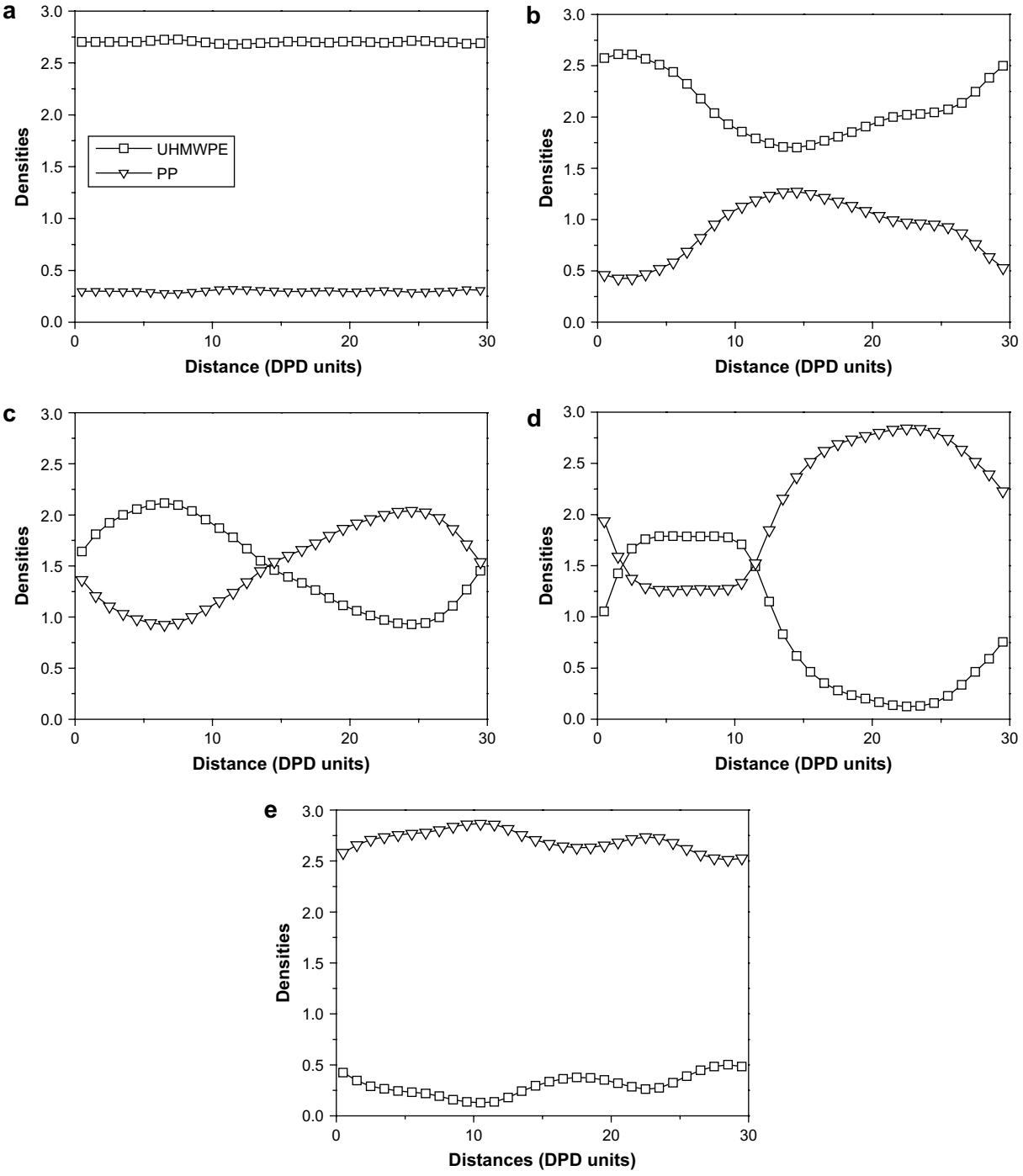

Fig. 2. Density profiles of the simulated blends UHMMPE/PP for (a) 90/10, (b) 70/30, (c) 50/50, (d) 30/70 and (e) 10/90.

3. Results and discussion

3.1. Mesoscopic morphology of UHMWPE/PP/PEG blends

Generally, the rheological behavior and processability of polymer blends strongly depend on their mesoscopic structure and state of dispersion-distribution [51,52]. For the UHMWPE/PP/PEG blends, we have investigated the effects of PP and PEG on the mesoscopic morphology by end-to-end distances of UHMWPE and density profiles of PP and PEG.

3.1.1. Effect of PP on mesoscopic morphology of the UHMWPE/PP/PEG blends

To analyze the effects of the concentration of PP on the mesoscopic morphology of the UHMWPE/PP/PEG ternary blends, first, we have investigated the binary UHMWPE/PP blends by varying the proportion of UHMWPE/PP from 90:10 to 10:90. Figs. 1 and 2 show the morphologies of the UHMWPE/PP blends and the corresponding density distribution of PP and UHMWPE beads obtained after 2×10^5 time steps DPD simulation. Apparently a totally disorder and homogeneous phase occurs when 10% of PP are added into UHMWPE, as shown in Fig. 1(a). There are hardly any fluctuations of densities distribution for UHMWPE and PP in the blends (see Fig. 2(a)) is totally consistent with Fig. 1(a). Therefore, the UHMWPE/PP (90/10) blends approximately possess a homogeneous phase at room temperature, leading to excellent mechanical properties, which is consistent with our previous studies [53].

As the concentration of PP increases, some different classical and nonclassical morphology appear. For example, spherical structure of PP formed in the UHMWPE/PP (70/30) blends with body-centered-cubic spheres (BCC) symmetry structure (see Fig. 1(b)). Our previous experimental investigations indicated that the viscosity of UHMWPE decreased obviously with an addition of 30% PP in the UHMWPE/PP (70/30) blends [54]. This probably should be attributed to the capability of spherical structures of PP to enhance the heat-transfer ability and induce the interphase slippage in the blends. As shown in Fig. 1(c), PP tends to form bicontinuous phase in the UHMWPE/PP (50/50) blends. The iso-density surface of PP divides the blends into PP-rich domain and the UHMWPE-rich domain (Figs. 1(c) and 2(c)).

At 70% concentration of PP, two phases including continuous phase of PP and stable perforated lamella (PL) structures of UHMWPE occur. An another interesting thing should also be mentioned here is that the perforations in the PL structures are always larger, more stable, and foursquare ordered, which is in agreement with S.F. César' results for polymer blends [55]. The time evolution of the morphology for the UHMWPE/PP blends was investigated by the DPD simulations to give a direct visualization of the underlying dynamic process, for which the phase separation of the UHMWPE/PP (30/70) blends was adopted as an example. Some

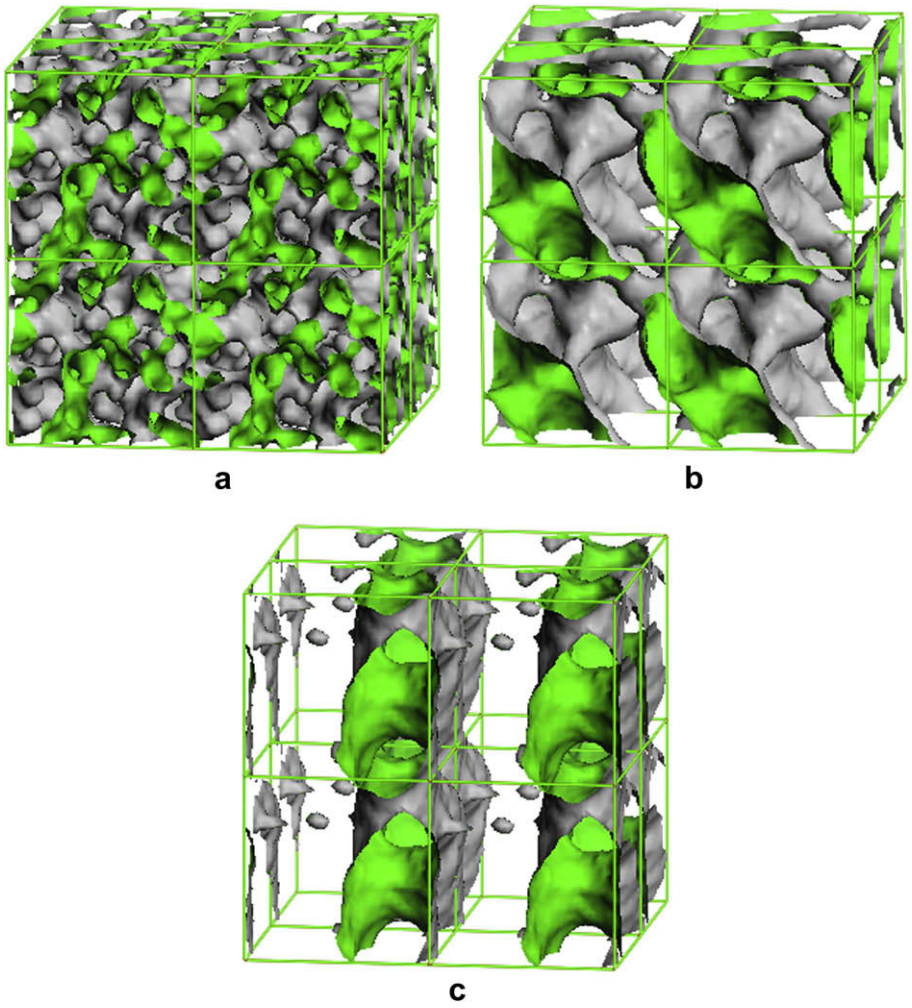

Fig. 3. Time evolution of iso-density surfaces of PP in the UHMMPE/PP (30/70) blends. The outward surfaces of PP phases are colored with green, and the rests are UHMMPE phases. Each system contains 8.1×10^4 DPD beads: (a) 1×10^3 steps, (b) 5×10^3 steps, and (c) 1×10^4 steps.

snapshots of the structures of the blends in the evolution process are given in Fig. 3. Details of the evolution process can be shown by a comparative scrutiny of Fig. 3 and Fig. 1(d). In Fig. 3(a), a structure of bicontinuous phase can be identified after 1×10^3 steps simulation. As shown in Fig. 3(b), which is plotted after 4×10^3 steps of Fig. 3(a), the bicontinuous phase becomes larger and more ordered gradually. In the next stage, the bicontinuous structures vanish, and PL structures of UHMWPE appear (Fig. 3(c)). At last this structure changes a little as time runs, and finally we obtain the two-phase structure as shown in Fig. 1(d). Figs. 3 and 1(d) reflect the dynamic

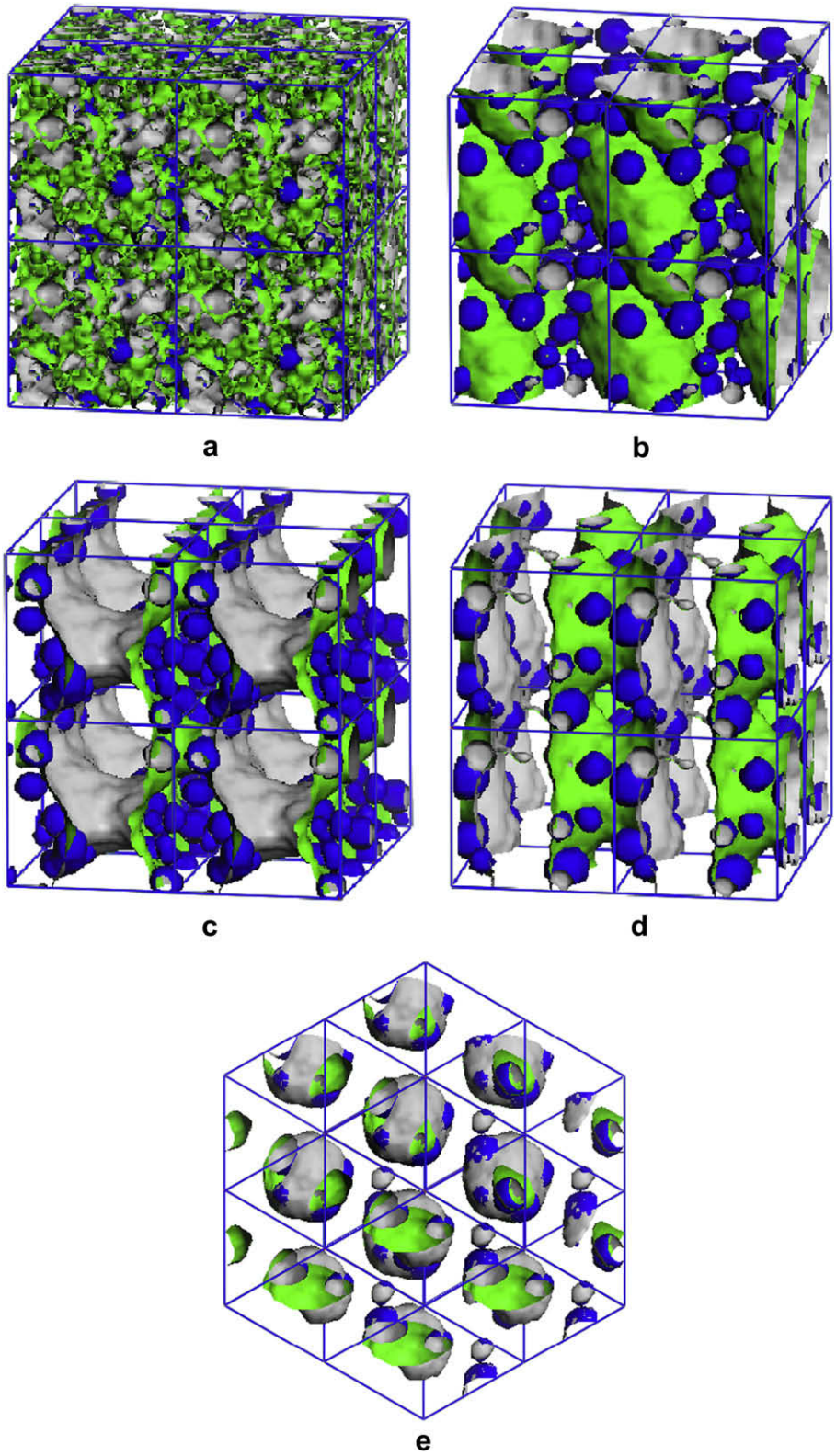

Fig. 4. Iso-density surfaces of PP and PEG for UHMMPE/PP blends obtained after 2×10^5 steps DPD simulation. The outward surfaces of PP phases are colored with green, the outward surfaces of PEG phases are colored with blue, and the rests are UHMMPE phases. Each system contains 8.1×10^4 DPD beads: (a) UHMMPE/PP (90/10/2), (b) 70/30/2, (c) 50/50/2, (d) 30/70/2 and (e) 10/90/2.

process that UHMWPE and PP are mixed together, whereas UHMWPE is excluded from PP to form UHMWPE-rich domains with the time increasing.

Between the totally disordered region and the ordered phases there are some melted structures, such as micelle-like. There is no symmetry in the phases, thus, we describe them as droplets (no matter large or small) of the minor moiety in disordered phases. Groot and Madden [19,32] distinguished processes on three different length and time scales in the formation of polymer mesophases: (1) phase separation on the mesoscopic bead level, (2) organization of polymers into micelles, and (3) the organization of these micelles into a superstructure with its own particular symmetry [19]. For the UHMWPE/PP (10/90) blends, a micelle-like phase is found between the disordered and BCC phases. This corresponds to the level (2) ordering in Groot and Madden's scheme.

Furthermore, DPD simulations of the effects of PEG on the morphologies of the UHMWPE/PP blends are performed by varying the concentrations of PP from 10 to 90. The concentration of PEG is 2 per hundred parts of UHMWPE/PP by weight (phr). The morphologies of the UHMWPE/PP/PEG blends and the corresponding density distribution of PP, PEG and UHMWPE particles obtained after 2×10^5 time steps DPD simulation are shown in Figs. 4 and 5. Obviously, PEG prefers to distribute in the phase of

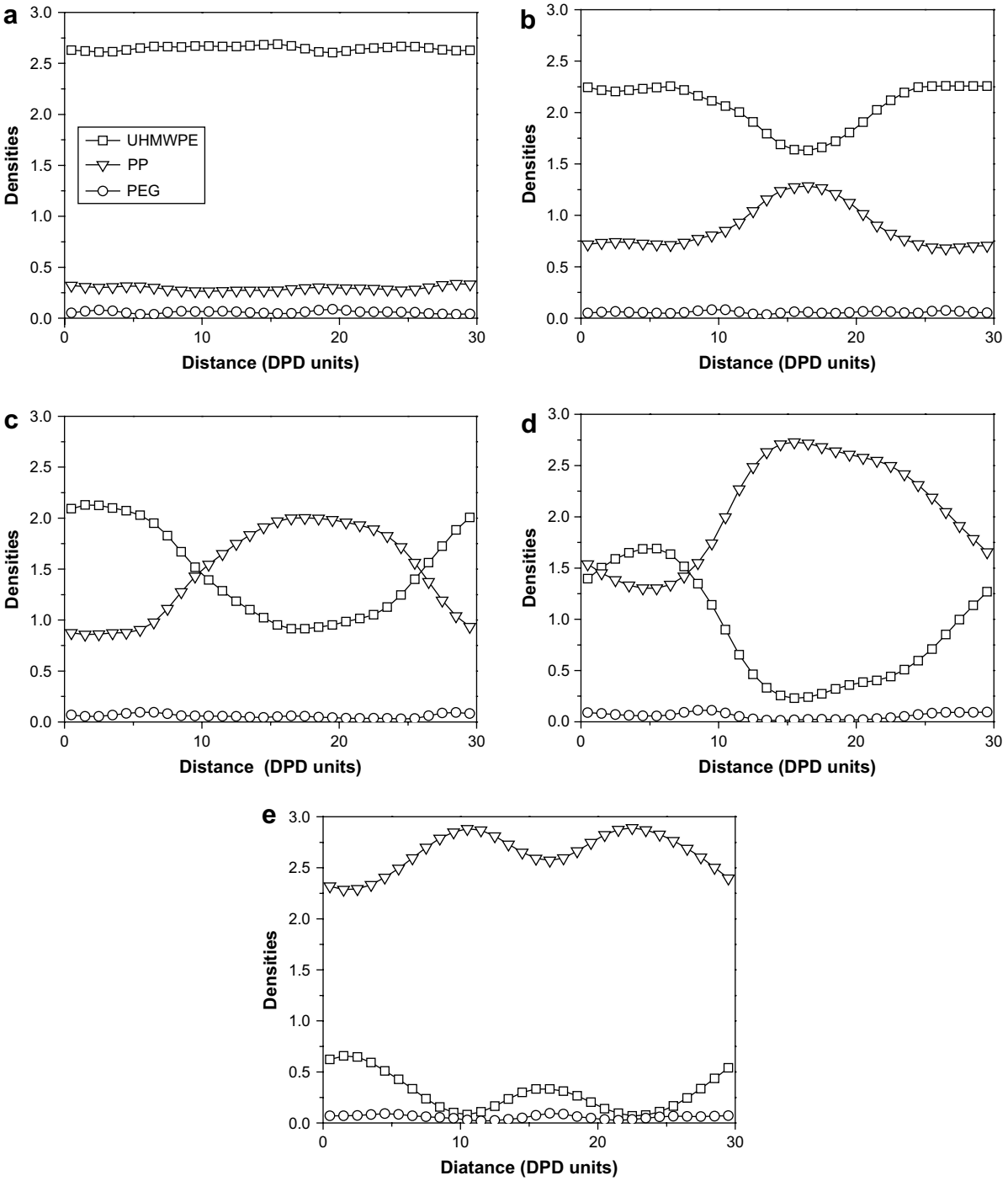

Fig. 5. Density profiles of the simulated UHMMPE/PP/PEG blends for: (a) 90/10/2, (b) 70/30/2, (c) 50/50/2, (d) 30/70/2 and (e) 10/90/2.

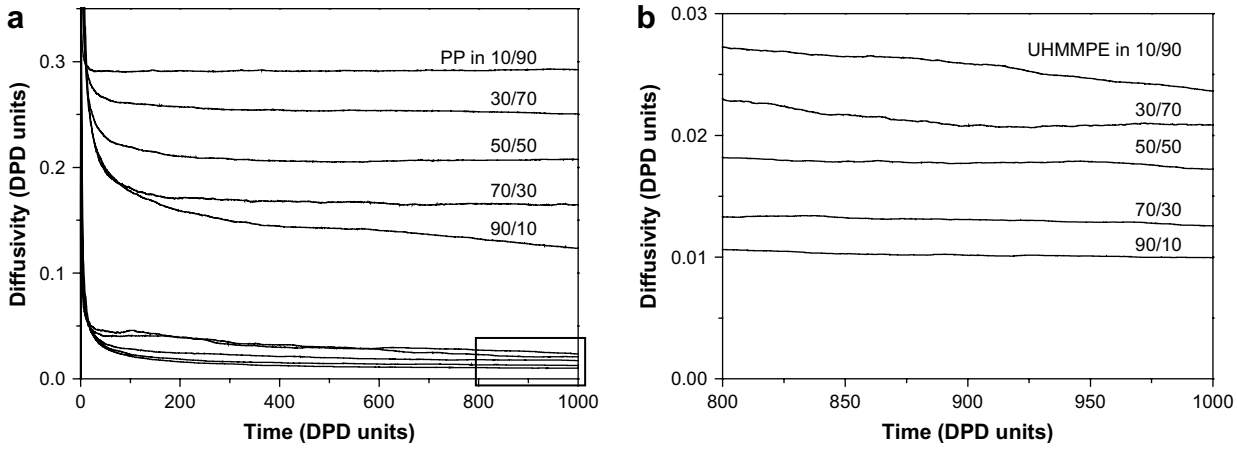

Fig. 6. Time evolution of diffusivities of PP and UHMMPE in the UHMMPE/PP blends with varying the proportion of the UHMMPE/PP blends from 90/10 to 10/90.

UHMWPE regardless of variation of PP concentration in UHMWPE/PP/PEG blends (see Figs. 4 and 5). By careful observation it was determined that PP in UHMWPE/PP/PEG blends exhibits morphology similar to that in the corresponding UHMWPE/PP blends (see Fig. 4(a)–(d)) except for the 10/90/2 blends, for which a hexagonal spheres morphology is observed (see Fig. 4(e)). Furthermore, the simulated density profiles of PP and UHMWPE Beads are also nearly identical to those of UHMWPE/PP (see Figs. 2 and 5). Due to the presence of an ether bond segments in PEG chains, UHMWPE and PP have very different polar character with PEG. Therefore, they would prefer to be located as far from each other as possible, leading to a phase separation of the ternary UHMWPE/PP/PEG systems. On the other hand, Flory–Huggins parameters $\chi_{UHMEPE/PEG}$ (0.191) estimated by Eq. (10) is much lower than $\chi_{PP/PEG}$ (0.412), which leads PEG to be concentrated more preferably in the phase of UHMWPE instead of PP.

3.1.2. Diffusivities of UHMWPE and PP for the UHMWPE/PP blends

Fig. 6 represents the changes in diffusivities of UHMWPE and PP with respect to a change in PP concentration in the UHMWPE/PP blends. The chain length of UHMWPE is larger than that of PP, and molecule diffusivity of PP is better than that of UHMWPE (see Fig. 6(a) and (b)). Hence, UHMWPE is easier to accumulate and separate phase than PP, which are directly demonstrated by the comparisons between Fig. 1(a) and (e), as well as between Fig. 1(b) and (d). Moreover, the diffusivities for both PP and UHMWPE increase with the increasing of PP concentration in the UHMWPE/PP blends (see Fig. 6(a) and (b)). Our previous experimental observations [54] showed that the melt apparent viscosity of the UHMWPE/PP blends decreased with the increase of PP content in the blends under all chosen temperature conditions, which might attribute to the enhancement of diffusivities for both PP and UHMWPE.

3.1.3. End-to-end distance of UHMWPE in the UHMWPE/PP blends

The end-to-end distance of polymer chains, which is calculated as a function of concentration of PP using the DPD simulations in the present study (Fig. 7), is an important structural property of polymer materials. It is evident that the end-to-end distances of UHMWPE molecules in the UHMWPE/PP blends decrease in the following order: $5.6977r_c$[UHMWPE/PP(100/0)] > $5.6277r_c$ (90/10) > $5.6056r_c$ (70/30) > $5.5348r_c$ (50/50) > $5.2266r_c$ (30/70) > $4.1507r_c$ (10/90)], which illustrates that the diameters of UHMEPE particles decrease with increasing the concentrations of PP. In the meanwhile, mesoscopic morphology of UHMWPE transits in the order: continuous phase (Fig. 1(a–c)), lamellae structure (Fig. 1(d)), and spherical structure (Fig. 1(e)), which is more in agreement with Fig. 7. Simulations of end-to-end distances give insight into the molecular-level details of the disentanglement response of UHMWPE to the concentrations of PP. Fig. 7 also illustrates the increase of disentanglement capability of PP for UHMWPE with increasing content of PP in the blends, which totally consists with the remarkable decrease of viscosity in our previous experimental observation [54].

3.2. Effect of shearing on the mesoscopic evolution of the UHMWPE/PP/PEG blends

The DPD simulations on the UHMWPE/PP/PEG (50/50/2) blends are performed, and the shear rates vary from 0.001 to 0.2. The simulated isosurfaces of both PP and PEG in the UHMWPE/PP/PEG (50/50/2) blends are shown in Fig. 8. When shear flow is added, the UHMWPE/PP/PEG (50/50/2) blends show very different morphologies as well as orientations, depending on the strength of shear flow (see Fig. 8). At a low shear rate of 0.001, the morphologies of both PP and UHMWPE are bicontinuous structures (see Fig. 8(a) and (b)), which is very similar with the morphology formed under the condition of no shear flow (Fig. 4(c)). Nevertheless, when the shear rate increases to 0.005, the bicontinuous structures disappear, and then lamellar morphologies occur, and the lamellar normal is not parallel to the velocity gradient direction (see Fig. 8(c)

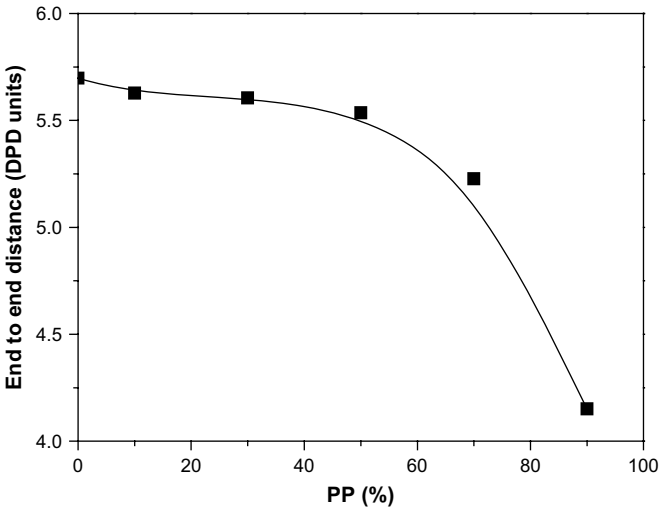

Fig. 7. Simulated dependence of end-to-end distance on PP concentrations varying from 10 to 90.

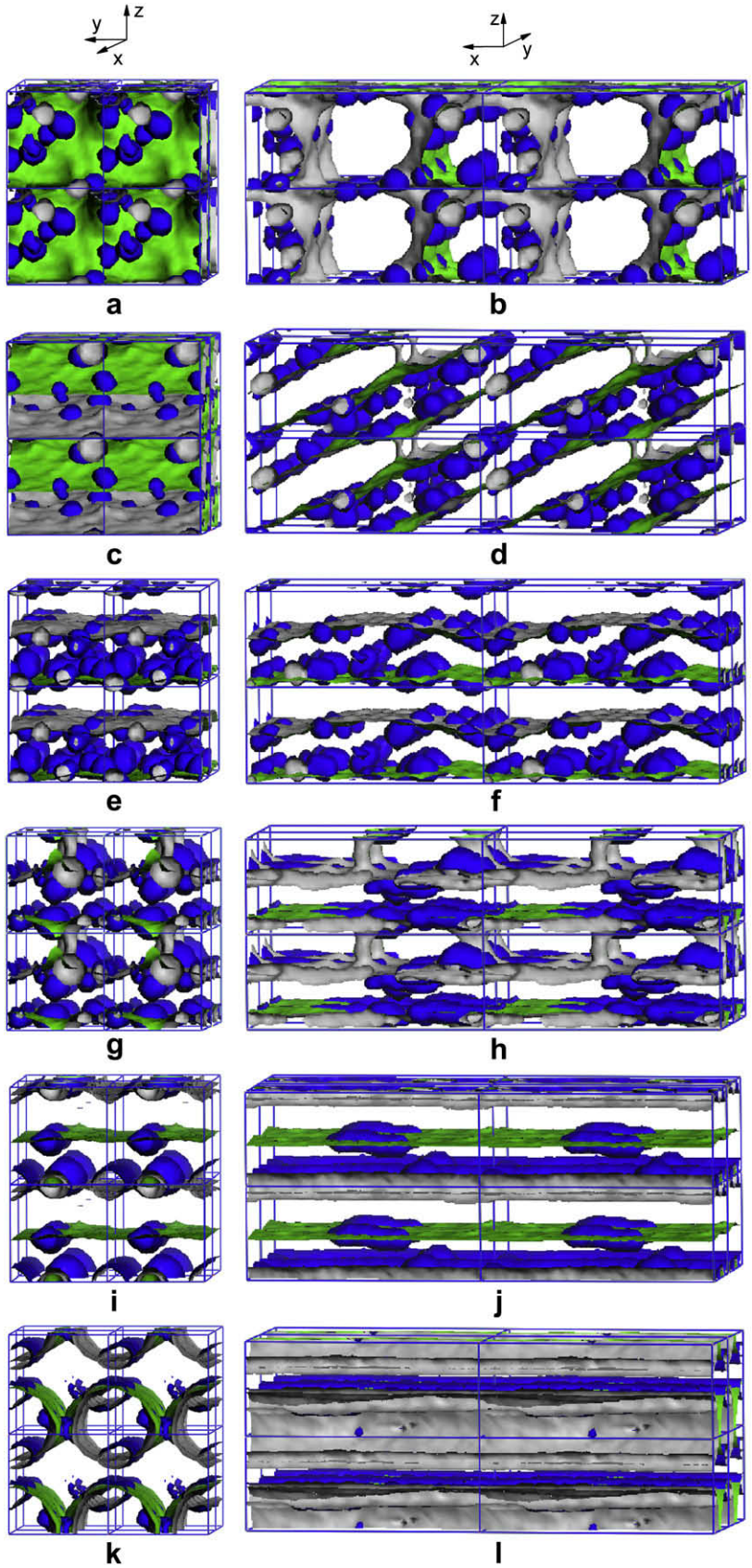

Fig. 8. Iso-density surfaces of PP and PEG for the UHMMPE/PP/PEG (50/50/2) blends obtained after 2×10^5 steps DPD simulation. The outward surfaces of PP phases are colored with green, the outward surfaces of PEG phases are colored with blue, and the rests are UHMMPE phases. Each system contains 6×10^4 DPD beads, *x*-axis is the shear flow direction: (a) and (b) 0.001 (shear rate), (c) and (d) 0.005, (e) and (f) 0.01, (g) and (h) 0.05, (i) and (j) 0.1, (k) and (l) 0.2. (For interpretation of the references to colour in this figure legend, the reader is referred to the web version of this article.)

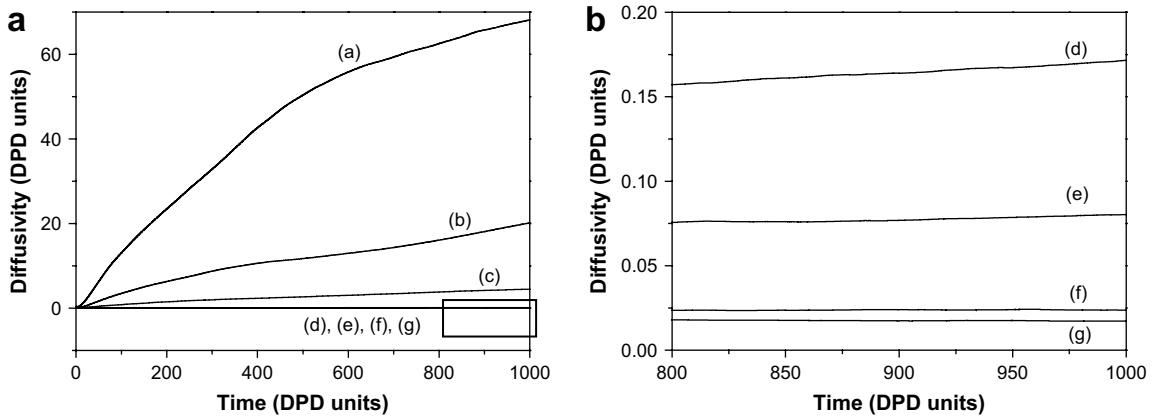

Fig. 9. Time evolution of diffusivities of UHMMPE in the UHMMPE/PP/PEG (50/50/2) blends with varying the shear rate: (a) 0.2, (b) 0.1, (c) 0.05, (d) 0.01, (e) 0.005, (f) 0.001 and (g) 0.0.

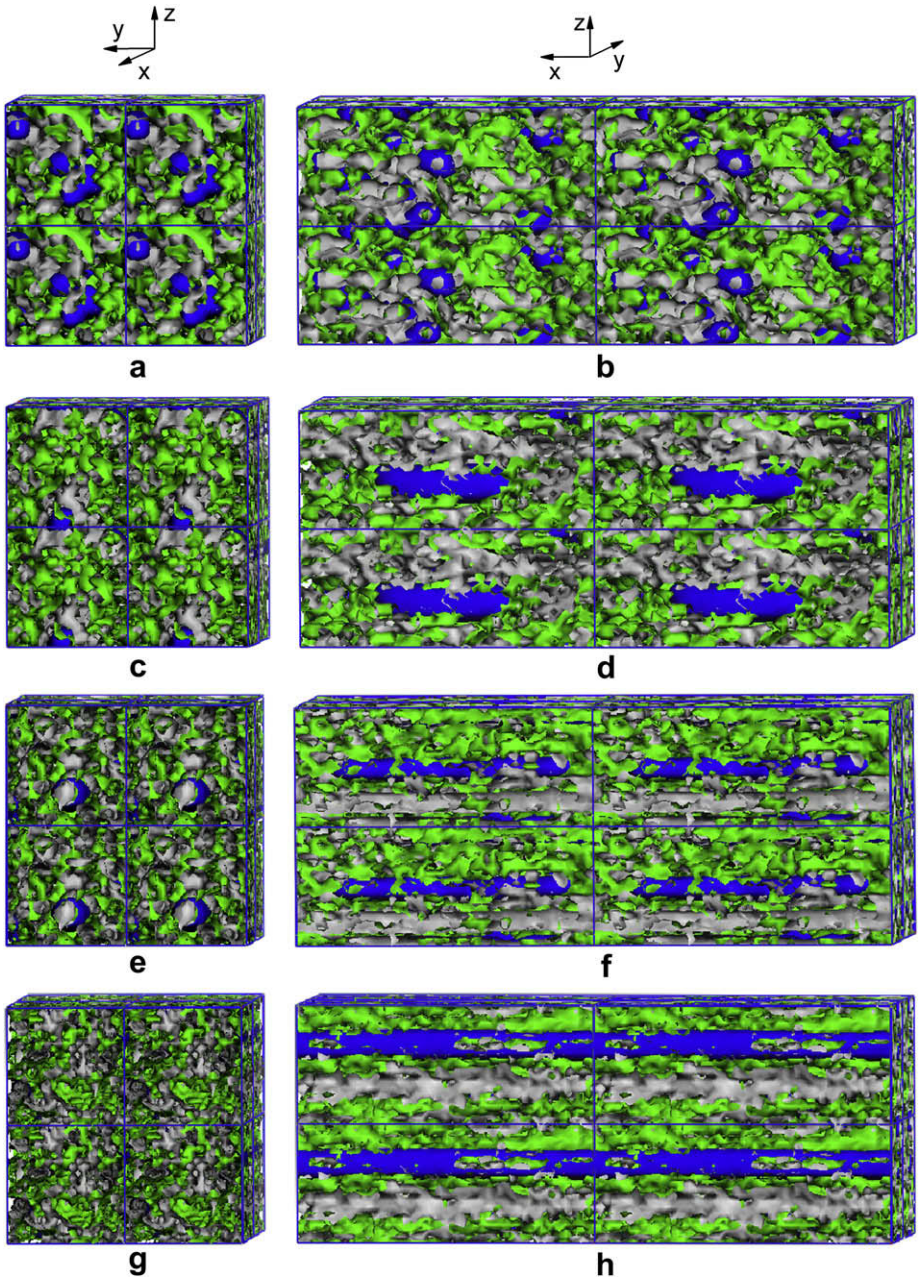

Fig. 10. Iso-density surfaces of PP and PEG for the UHMMPE/PP/PEG (90/10/2) blends obtained after 2×10^5 steps DPD simulation. The outward surfaces of PP phases are colored with green, the outward surfaces of PEG phases are colored with blue, and the rests are UHMMPE phases. Each system contains 6×10^4 DPD beads, *x* axis is the shear flow direction: (a) and (b) 0.01 (shear rate), (c) and (d) 0.05, (e) and (f) 0.1, (g) and (h) 0.2. (For interpretation of the references to colour in this figure legend, the reader is referred to the web version of this article.)

and (d)). Within the shear rate of 0.01–0.1, both PP and UHMWPE in the UHMWPE/PP/PEG (50/50/2) blends always gives parallel lamellar alignment, whose normal is parallel to the velocity gradient direction (see Fig. 8(e)–(j)), whereas the blends show cylindrical morphology with shear rate of 0.2 (see Fig. 8(k) and (l)).

From Fig. 8, it can be seen that PEG in the UHMWPE/PP/PEG (50/50/2) blends turns into a spherical structure and concentrates more in the UHMWPE phase under the condition of shear rate from 0.0 to 0.01 (see Fig. 4(c) and Fig. 8(a)–(f)). When the shear rate increases to 0.05, PEG particles localize preferably in the interface between PP and UHMWPE phases, and ellipsoidal and discontiguous cylindrical morphology appear gradually, as shown in Fig. 8(g) and (h). For the shear rate of 0.1, PEG totally concentrated about interfaces with contiguous cylindrical and a small quantity of ellipsoidal morphologies (Fig. 8(i) and (j)). At a high shear rate of 0.2, PEG totally forms with cylindrical morphologies, and concentrates mostly in PP phase with only a part locating between two cylindrical PP phases (Fig. 8(k) and (l)). In conclusion, with the increasing of shear flow, PEG phase translates preferably from UHMWPE phase to PP phase, which probably is attributed to two reasons: (1) Flory–Huggins parameters [$\chi_{UHMEPE/PEG}$ (0.191) < $\chi_{PP/EG}$ (0.412)] dominate the location of PEG at a low shear rates; (2) the obviously closer viscosity of PEG to that of PP than that of UHMWPE forms the main factor at a high shear rates.

The simulated diffusivities of UHMWPE for the UHMWPE/PP/PEG (50/50/2) as a function of shear rate are shown in Fig. 9. It is evident that the diffusivity of UHMWPE increases with increasing shear rate (Fig. 9), which illustrates that the viscosities of the blends decrease to a certain extent under shear flow. When the shear rate is higher than 0.05, the diffusivities of UHMWPE increase rapidly (Fig. 9). Our previous experimental investigations on the UHMWPE/PP/PEG blends showed that shear thinning appears at higher shear rates, and the blends exhibit a non-Newtonian behavior [56], which probably should be attributed to the increasing of diffusivities for UHMWPE in the blends. Interestingly, it is found that at low shear rates the diffusivities are almost independent of shear rates for the UHMWPE/PP/PEG (50/50/2) blends (Fig. 9), which probably implies that they all exhibit a Newtonian behavior in this region.

DPD simulations for a large amount of UHMWPE in blends have been further performed by varying shear rate from 0.01 to 0.2. In the case of the UHMWPE/PP/PEG (90/10/2) blends, as shown in Fig. 10, the distributions of PP and UHMWPE are totally disordered and homogeneous throughout the considered shear rates. Luckily, the morphologies of PEG are more sensitive to shear rates, and spherical and cylindrical morphology occur in turn with the increasing of shear rates (Fig. 10(a)–(h)). It is well known that PEG has very low viscosity and good lubricating property. PEG with spherical and cylindrical morphologies in the UHMWPE/PP (90/10) blends might act as a lubricant to induce interphase slippage of the blends.

4. Conclusions

In this paper, the DPD method is used to investigate the mesoscopic morphologies and properties of binary UHMWPE/PP and ternary UHMWPE/PP/PEG blends. As composition of the blends varied, the mesoscale simulations have predicted the ordered structures with defined morphology of lamellae, perforated lamellae, hexagonal spheres, and body-centered-cubic spheres as well as micelle-like melted structures. For the UHMWPE/PP/PEG blends, we have investigated the effects of PP and PEG on the mesoscopic morphology by end-to-end distances of UHMWPE and density profiles of PP and PEG. PEG prefers to distribute in the phase of UHMWPE regardless of variation of PP concentrations. It is evident that the end-to-end distances of UHMWPE molecule in the UHMWPE/PP blends decrease with the increasing of PP concentrations, which illustrates that the diameters of UHMEPE particles decrease with increasing concentration of PP. When the shear rate is higher than 0.05, the diffusivities of UHMWPE increase rapidly. Our previous experimental investigations on the UHMWPE/PP/PEG blends showed that shear thinning appears at higher shear rates, and the blends exhibit a non-Newtonian behavior, which probably attributes to the increase of diffusivities for UHMWPE in the blends. Information about their mesoscopic morphology can further be employed in designing new materials for advanced technology applications.

Acknowledgements

This work was supported by the National Basic Research Program of China (2005CB623800).

References

[1] Engh CA, Massin P. Clin Ortho Relat Res 1989;24:141.
[2] Kumar P, Oka M, Ikeuchu K, Shimizu K, Yamamuro T, Okumura H, et al. J Biomed Mater Res 1991;25:813.
[3] Prever EB, Crova M, Costa L, Dallera A, Camino G, Gallinaro P. Biomaterials 1996;17:873.
[4] Furmanski J, Pruitt LA. Polymer 2007;48:3512.
[5] Ranade RA, Wunder SL, Baran GR. Polymer 2006;47:4318.
[6] Smith P, Lemstra PJ. Makromol Chem 1979;180:2983.
[7] Smith P, Lemstra PJ. Polymer 1980;21:1341.
[8] Ivan'kova EM, Krumova M, Myasnikova LP, Marikhin VA, Michler GH. Polymer 2006;47:5623.
[9] Ruan SL, Gao P, Yu TX. Polymer 2006;47:1604.
[10] Dumoulin MM, Utracki LA, Lara J. Polym Eng Sci 1984;24:117.
[11] Kyu T, Vadhar P. J Appl Polym Sci 1986;32:5575.
[12] Liu GD, Li HL. J Appl Polym Sci 2003;89:2628.
[13] Xie MJ, Liu XL, Li HL. J Appl Polym Sci 2006;100:1282.
[14] Li SN, Liu Y, Tuo XL, Wang XG. Polymer 2008;49:2775.
[15] Huang CI, Yu HT. Polymer 2007;48:4537.
[16] Huang CI, Chiou YJ, Lan YK. Polymer 2007;48:877.
[17] Koelman JMVA, Hoogerbrugge PJ. Europhys Lett 1993;21:363.
[18] Groot RD, Warren PB. J Chem Phys 1997;107:4423.
[19] Groot RD, Madden TJ. J Chem Phys 1998;108:8713.
[20] Zhang K, Manke CW. Comput Phys Commun 2000;129:275.
[21] Spenley NA. Europhys Lett 2000;49:534.
[22] Liu DH, Zhong CL. Macromol Rapid Commun 1960;2005:26.
[23] Hoogerbrugge PJ, Koelman JMVA. Europhys Lett 1992;19:155.
[24] Español P, Warren PB. Europhys Lett 1995;30:191.
[25] Kong Y, Manke CW, Madden WG, Schlijper AG. Int J Thermophys 1994;15:1093.
[26] Schlijper AG, Hoogerbrugge PJ, Manke CW. J Rheol 1995;39:567.
[27] He YD, Qian HJ, Lu ZY, Li ZS. Polymer 2007;48:3601.
[28] Lee WJ, Ju SP, Wang YC. J Chem Phys 2007;127:064902.
[29] Yang H, Li ZS, Lu ZY, Sun CC. Eur Polym J 2005;41:2956.
[30] Anastasiadis SH, Ganzarz I, Koberstein JT. Macromolecules 1988;21:2980.
[31] Kong Y, Manke CW, Madden WG. J Chem Phys 1997;107:592.
[32] Groot RD, Madden TJ, Tildesley DJ. J Chem Phys 1999;110:9739.
[33] Jury S, Bladon P, Cates M, Krishna S, Hagen M, Ruddock N, et al. Phys Chem Chem Phys 1999;1:2051.
[34] Clark AT, Lal M, Ruddock JN, Warren PB. Langmuir 2000;16:6342.
[35] Shillcock JC, Lipowsky R. J Chem Phys 2002;117:5048.
[36] Rekvig L, Kranenburg M, Vreede J, Hafskjold B, Smit B. Langmuir 2003;19:8195.
[37] Tsige M, Grest GS. J Chem Phys 2004;120:2989.
[38] Wijmans CM, Smit B, Groot RD. J Chem Phys 2001;114:7644.
[39] Groot RD, Rabone KL. Biophys J 2001;81:725.
[40] Hildebrand JH. The solubility of non-electrolytes. New York: Reinhold; 1936.
[41] Case FH, Honeycutt JD. Trends Polym Sci 1994;2:256.
[42] Liu DH, Zhong CL. Macromol Rapid Commun 2006;27:458.
[43] Groot RD. J Chem Phys 2003;118:11265.
[44] Özen AS, Sen U, Atilgan C. J Chem Phys 2006;124:064905.
[45] Liu DH, Zhong CL. Polymer 2008;49:1407.
[46] Materials Studio V 4.0. San Diego, CA: Accelrys Inc.; 2005.
[47] Rubinstein M, Colby RH. Polymer physics. Oxford University Press; 2003.
[48] Help of Materials Studio V 4.0. San Diego, CA: Accelrys Inc.; 2005.
[49] Jawalkar SS, Aminabhavi TM. Polymer 2006;47:8061.
[50] Rogers D, Hopfinger AJ. J Chem Inf Comput Sci 1994;34:854.
[51] Ray SS, Maiti P, Okamoto M, Yamada K, Ueda K. Macromolecules 2002;35:3104.
[52] Sinha RS, Okamoto K, Okamoto M. Macromolecules 2003;36:2355.
[53] Gai JG, Li HL. J Appl Polym Sci 2007;106:3023.
[54] Liu GD, Chen YZ, Li HL. J Appl Polym Sci 2004;92:3894.
[55] César SF, Luis V. Polymer 2007;48:3902.
[56] Xie MJ, Li HL. Eur Polym J 2007;43:3480.